We are IntechOpen,
the world's leading publisher of Open Access books
Built by scientists, for scientists

4,800
Open access books available

122,000
International authors and editors

135M
Downloads

Our authors are among the

154
Countries delivered to

TOP 1%
most cited scientists

12.2%
Contributors from top 500 universities

BOOK CITATION INDEX
CLARIVATE ANALYTICS
INDEXED

WEB OF SCIENCE™

Selection of our books indexed in the Book Citation Index
in Web of Science™ Core Collection (BKCI)

Interested in publishing with us?
Contact book.department@intechopen.com

Epitaxial Electrodeposition of Chiral Films Using Chiral Precursors

Rakesh Gudavarthy and Elizabeth A. Kulp

Additional information is available at the end of the chapter

1. Introduction

Chiral drugs have played an important role in driving the market for past few decades. Currently, more than half of the drugs marketed are chiral. [1-4] It is well established that chiral drugs often differ in their pharmacological, toxicological and pharmacokinetic properties. Historically, the pharmaceutical industry has relied on using enzymatic reactions to produce enantiospecific molecules. The chiral drugs are often synthesized in the racemic form, and are then resolved into pure enantiomer. [5] From an Industry perspective, the process is neither cost effective nor completely safe. The enantiomer should be characterized in detail in order to develop a safe and reliable formulation. One way to get around that would be to develop enantiospecific catalyst that can be reused. Chiral surfaces offer this possibility. They have been produced by decorating the surfaces of achiral substrates by chiral molecules, or by introducing defects in the single crystals which exposes chiral kink sites. [6-17] It was shown that chiral surfaces can also be produced by electrodeposition technique. [18, 19] Unlike other vacuum techniques, electrodeposition is cheaper and can be carried out at ambient conditions. [20, 21] In this method, chiral molecules present in the electrodeposition solution determine the final Chirality of the electrodeposited thin film. In this regard, electrodeposition resembles biomineralization, where organic molecules adsorbed on surface, reduce the symmetry of surfaces, resulting in chiral crystal habits. [22-28] Crystals like calcite and gypsum which crystallize in achiral space group can be transformed to chiral space group by treating calcite with chiral etchants or by crystallizing calcite in the presence of amino acids. Chiral morphologies of calcites can also be deposited electrochemically. [29]

In this chapter the terms and concepts employed in describing the enantiospecific electrodeposition are introduced. In addition, before embarking on a detailed consideration of methods of studying chiral deposition process and the various characterization techniques, we will try to understand the techniques involved in the preparation and characterization of these films.

2. Chirality

A chiral structure is non-superimposable on its mirror image. Pasteur reported in 1984 the concept of the molecular Chirality based on the distinction between the configurational isomers of molecules. Configurational isomers are compounds with the same molecular formula and same groups but different configurations. Enantiomers are pairs of configurational isomers that are mirror images of each other but are non-superimposable. Diastereomers are pairs of compounds that contain more than one chiral center, not all of which are superimposable. An equimolar mixture of opposite enantiomers is called racemic mixture or a racemate. Enantiomers when exposed to polarized light behave differently and have different catalyzing properties in a chiral medium. On the other hand, the racemic mixtures have completely different properties than enantiomers. The difference in the properties between the enantiomers and racemic mixtures arise due to different molecular interactions, and different crystal structures. [30, 31]

In an enantiomer, the molecular interactions are homochiral, which are the interactions between the assemblies of molecules with same Chirality. In a racemic compound the interactions are heterochiral, where the interactions are between opposite chiral molecules. The difference between the homochiral and heterochiral interactions leads to different physical properties. Particularly in a racemic compound, because the unit cell consists of enantiomeric molecules with opposite Chirality, the properties are completely different from enantiomers. Racemic compounds are the most common compounds that occur in nature. Such racemic compounds can exist in different forms based on the intermolecular interactions in their crystals. Analysis of the crystal structures facilitates enormously our understanding of the factors that determine the various physical and chemical properties, such as the thermodynamic stability of different types of racemates. [32] The details of such analysis are beyond the scope of this chapter.

Due to the presence of various chiral compounds, it is critical to have the right nomenclature for the differentiation. The internationally accepted nomenclature for chiral molecules uses the Cahn-Ingold-Prelog (CIP) rules for sp3 carbons. The four substituents are sorted by increasing mass of the first atom attached to the asymmetric center. If two atoms are identical, the next heaviest atom one bond further away is considered and so on. For example, in the case of 2-butanol with the order OH →ethyl → methyl rotating clockwise will be a R-enantiomer and the mirror image of that will be a S-enantiomer. These rules allow us for the absolute configuration of any chiral compounds. Another accepted form for nomenclature is Dextro (D-) and Levo (L-), based on the optical rotation of the compound. Setting glycine apart since it is nonchiral, it must be noted that all amino acids found in proteins are L-amino acids and also have the S-configuration at the exception of cysteine whose -CH2-SH substituent precedes the carboxylate -COOH in mass making L-cysteine the R-enantiomer. It is interesting to note that the electrodeposited chiral films also follow the CIP rules. It was shown that the CuO films grown from both R versions of tartaric acid and malic acid resulted in (1-1-1) orientation on Cu(111), while the S version of each resulted in a (-111) mirror image. [33] However, there are exceptions for films grown from amino acids which will be discussed in detail.

3. Chirality in crystals

The Chirality of a crystal depends on the symmetry operations present in the structure. Proper symmetry operations are those that do not change the handedness of an object. These operations include rotation axes, translations, and screw axes. If an object can be rotated about an axis and repeats itself after being rotated through either 360, 180, 120, 90 or 60° is said to have an axis of 1-fold, 2-fold, 3- fold, 4-fold, or 6-fold rotational symmetry. Although objects themselves may appear to have 5-fold, 7-fold, 8-fold or higher-fold rotation axes, these are not possible in crystals. The reason is that the external shape of a crystal is based on a geometric arrangement of atoms.   In a translation operation, the object is translated up or down along an axes. Where as a screw axis also referred to as twist axis of an object are the axes that are simultaneously the axis of rotation and the axis along which a translation occurs. These symmetry operations do not change the original object because they are just movements of the same object. If only these operations are present, then the structure is chiral. However, improper symmetry operations such as rotoinversion operations or glide reflection produce the opposite "hand" of the object. [34] A rotoinversion operation is a combination of rotation and inversion where as the glide reflection is a combination of reflection and translation operation along a line. Any structure with one of these symmetery operators will produce an achiral structure.

The symmetry of the system determines what planes of a material are chiral. In the case of copper(II) oxide CuO (focus material in this chapter), the lattice parameters are a = 0.4685 nm, b = 0.3430 nm, c = 0.5139 nm, $\alpha = \Upsilon = 90°$, and $\beta = 99.08°$. The structure is centrosymmetric (i.e. it has an inversion center, i); therefore, the bulk crystal structure of CuO is achiral. However, crystallographic orientations/planes may be chiral. A monoclinic system has three axes of unequal length and an angle normally greater than 90o between two axes. In this arrangement, the b'axis is unique. The c and a axes do not intersect each other at right angles, but they are perpendicular to the b-axis. Based on the space group, a glide plane has a mirror or glide plane perpendicular to it. Therefore, achiral planes of CuO are planes that are parallel to the b-axis, planes k=0. Thus, planes such as (101), (001), and (102) are achiral. Chiral CuO planes lack glide plane symmetry; chiral planes are those with k ≠ 0, such as (111), (110), (022), and (020). For a chiral plane (hkl), its enantiomer is (-h-k-l).

Table 1 lists the symmetry of specific planes depending on the point group. [35] Screw axes are replaced by the highest possible rotation, and glides are replaced by mirrors. Planes that lack mirror symmetry (m) are chiral. For example, whereas all planes of triclinic structure are chiral, all planes of orthorhombic structure are achiral except where h≠k≠l≠0, the space group of CuO is C2/c; its point group is 2/m. According to table 1, chiral planes are {010}, {0kl}, {hk0}, and {hkl}, whereas achiral planes are {100}, {001}, and {h01}. From these select planes, a trend is visible; achiral planes are those that k=0. This trend is true for all monoclinic structures.

System	Space Group	Point Group	{100}	{010}	{001}	{0kl}	{h0l}	{hk0}	{hkl}
Triclinic	1	1	1	1	1	1	1	1	1
	2	$\bar{1}$	2	2	2	2	2	2	2
Monoclinic (2nd setting)	3-5	2	m	2	m	1	m	1	1
	6-9	m	m	1	m	1	m	1	1
	10-15	2/m	2mm	2	2mm	2	2mm	2	2
Ortho-rhombic	16-24	222	2mm	2mm	2mm	m	m	m	1
	25-46	mm2	m	m	2mm	m	m	m	1
		m2m	m	2mm	m	m	m	m	1
		2mm	2mm	m	m	m	m	m	1
	47-74	mmm	2mm	2mm	2mm	2mm	2mm	2mm	2

System	Space Group	Point Group	{001}	{100}	{110}	{hk0}	{h0l}	{hhl}	{hkl}
Tetragonal	75-80	4	4	m	m	m	1	1	1
	81-82	$\bar{4}$	4	m	m	m	1	1	1
	83-88	4/m	4	2mm	2mm	2mm	2	2	2
	89-98	422	4mm	2mm	2mm	m	m	m	1
	99-110	4mm	4mm	m	m	m	m	m	1
	111-122	$\bar{4}$2m	4mm	m	2mm	m	m	m	1
	123-142	$\bar{4}$m2	4mm	2mm	2mm	2mm	2mm	2mm	2

System	Space Group	Point Group	{001}	{100}	{110}	{hk0}	{h0l}	{hhl}	{hkl}
Trigonal (hexagonal axes)	143-146	3	3	1	1	1	1	1	1
	147-148	$\bar{3}$	6	2	2	2	2	2	2
	149-155	321	31m	m	2	1	m	1	1
		312	3m1	2	m	1	1	m	1
	156-161	3m1	3m1	m	1	1	m	1	1
	162-167	$\bar{3}$m1	6mm	2mm	2	2	2mm	2	2
		$\bar{3}$1m	6mm	2	2mm	2	2	2mm	2
Hexagonal	168-173	6	6	m	m	m	1	1	1
	174	$\bar{6}$	3	m	m	m	1	1	1
	175-176	6/m	6	2mm	2mm	2mm	2	2	2
	177-182	622	6mm	2mm	2mm	m	m	m	1
	183-186	6mm	6mm	m	m	m	m	m	1
	187-190	$\bar{6}$m2	3m1	2mm	m	m	m	m	1
		$\bar{6}$2m	31m	m	2mm	m	m	m	1
	191-194	6/mmm	6mm	2mm	2mm	2mm	2mm	2mm	2

System	Space Group	Point Group	{100}	{111}	{110}	{hk0}	{hhl} h>l	{hhl} h<l	{hkl}
Cubic	195-199	23	2mm	3	m	m	1	1	1
	200-206	m3	2mm	6	2mm	2mm	2	2	2
	207-214	432	4mm	3m	m	m	m	m	1
	215-220	$\bar{4}$3m	4mm	3m	m	m	m	m	1
	221-230	m3m	4mm	6mm	2mm	2mm	2mm	2mm	2

Table 1. Symmetry of the planes of a point group. Orientations that lack mirror symmetry (i.e. having rotational symmetry) are chiral. The chiral orientations are highlighted in yellow.

Other methods to determine whether a surface is chiral or achiral are stereographic projections and interface models. Like a point group, stereographic projections is a two-dimensional plot that shows the angular relationships of the crystal's planes and directions based on its crystallographic symmetry. Simply, a stereographic projection is a way to represent a three dimensional crystal on a two dimensional page. If two orientations have a stereographic projections that are superimpossible mirror images, then the orientations are achiral. If the two orientations produce stereographic projections that are nonsuperimposable mirror images, then the orientations are chiral.

Calculated stereographic projections are shown in figure 1 for the achiral planes (001) and (00-1) of CuO and in figure 2 for the chiral planes (111) and (-1-1-1) of CuO. In figure 1 A and 1B, the stereographic projections of the (001) and (00-1) planes are superimposable mirror images of each other. In addition, each projection has mirror symmetry. This mirror symmetry in the stereographic projection indicates that there is an improper symmetry operator perpendicular to this surface, resulting in planes that are achiral. In figure 2A and 2B, although the stereographic projections of the (111) and (-1-1-1) planes are mirror images of each other, they are not superimposable. Also, neither projection has mirror symmetry. The absence of mirror symmetry in the stereographic projection indicates that only proper symmetry operators are perpendicular to this surface. The presence of only symmetry operators indicates that these planes are chiral.

Thus based on the structure and orientation of the thin films, one can determine whether or not the film is chiral.

4. X-ray Diffraction characterization of Films

X-ray diffraction (XRD) is a non-destructive technique that reveals crystallography of an unknown material using monochromatic X-rays. X-rays are generated by an X-ray tube that uses a high voltage to accelerate the electrons released by a cathode to a high velocity. The so generated electrons collide with a metal target, the anode, creating the X-rays. [36] Different X-ray sources are used based on the need. Tungsten or a crack-resistant alloy of rhenium (5%) and tungsten (95%) are generally used in the medical field. When soft X-rays are needed for special applications like mammography, a molybdenum source is used. In crystallography, a copper target is most common, with cobalt often being used when fluorescence from iron content in the sample might otherwise present a problem. For a copper target, X-ray emissions commonly contains a continuous white radiation and two characteristic x-rays, Kα (λ = 0.15418 nm) and Kβ (λ = 0.13922 nm) leading from 2p $\rightarrow$1s and 3p $\rightarrow$1s transitions, respectively. In general, the Kα transition is more intense than Kβ, and is a combination of Kα1 and Kα2. This is because of the slight difference between two possible spin states of 2p electrons. Monochromatic Kα X-rays can be obtained by using suitable filters that absorb the unneeded white radiation and Kβ. For example, a Ni foil is commonly used for radiation of copper target. [37]
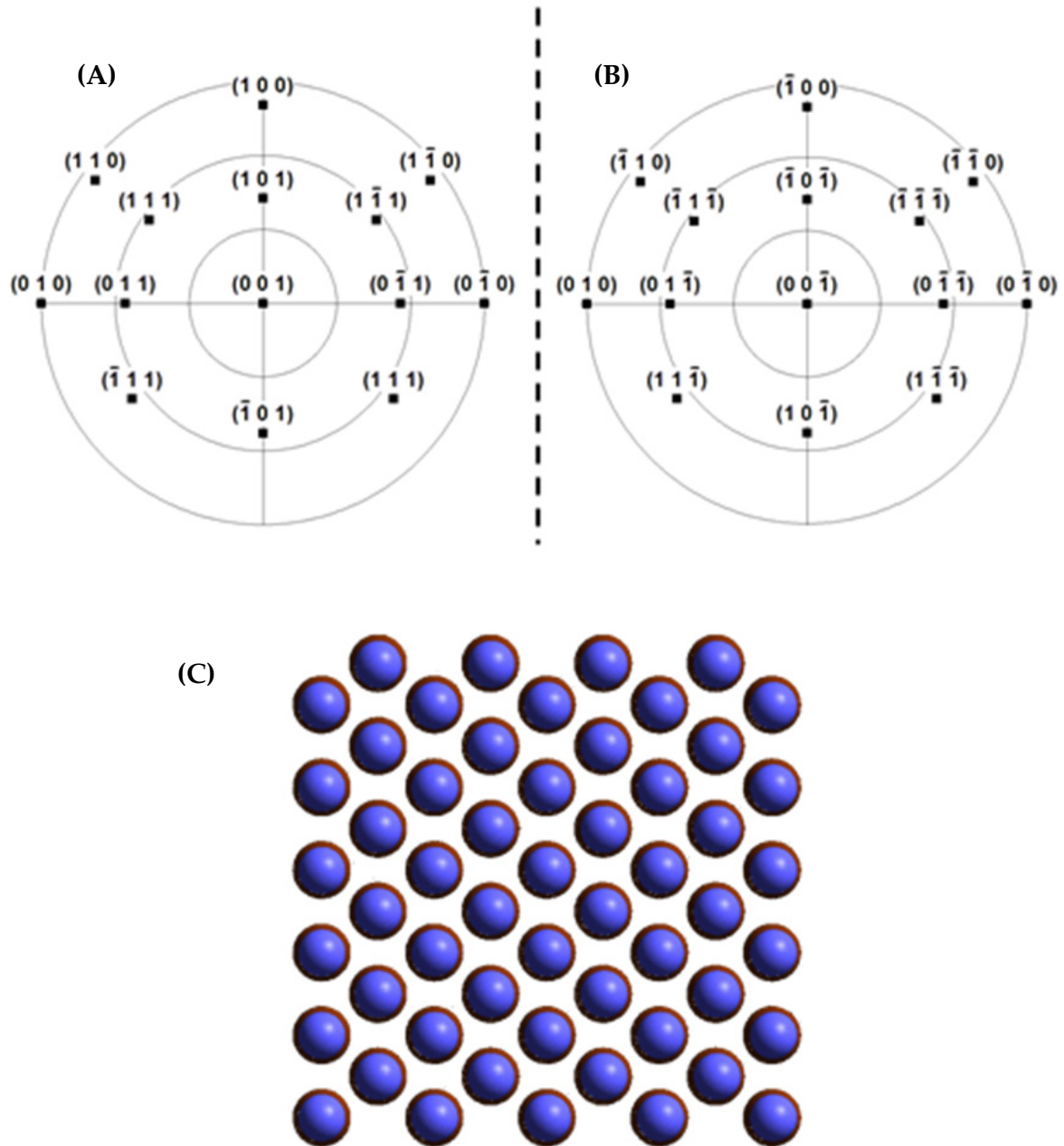
Figure 1. Stereographic projections of the A) (001) and B) (00-1) orientations of CuO. These two orientations are superimposable mirror images of each other; they are achiral. The radial grid lines on the stereographic projections correspond to 30° increments of the tilt angle, χ. C) the interface model of (00-1) CuO (front, blue Cu atoms) on (001) CuO (back, brown Cu atoms) with a common [010] directions. These two orientations are superimposed onto each other, indicating that they are achiral.
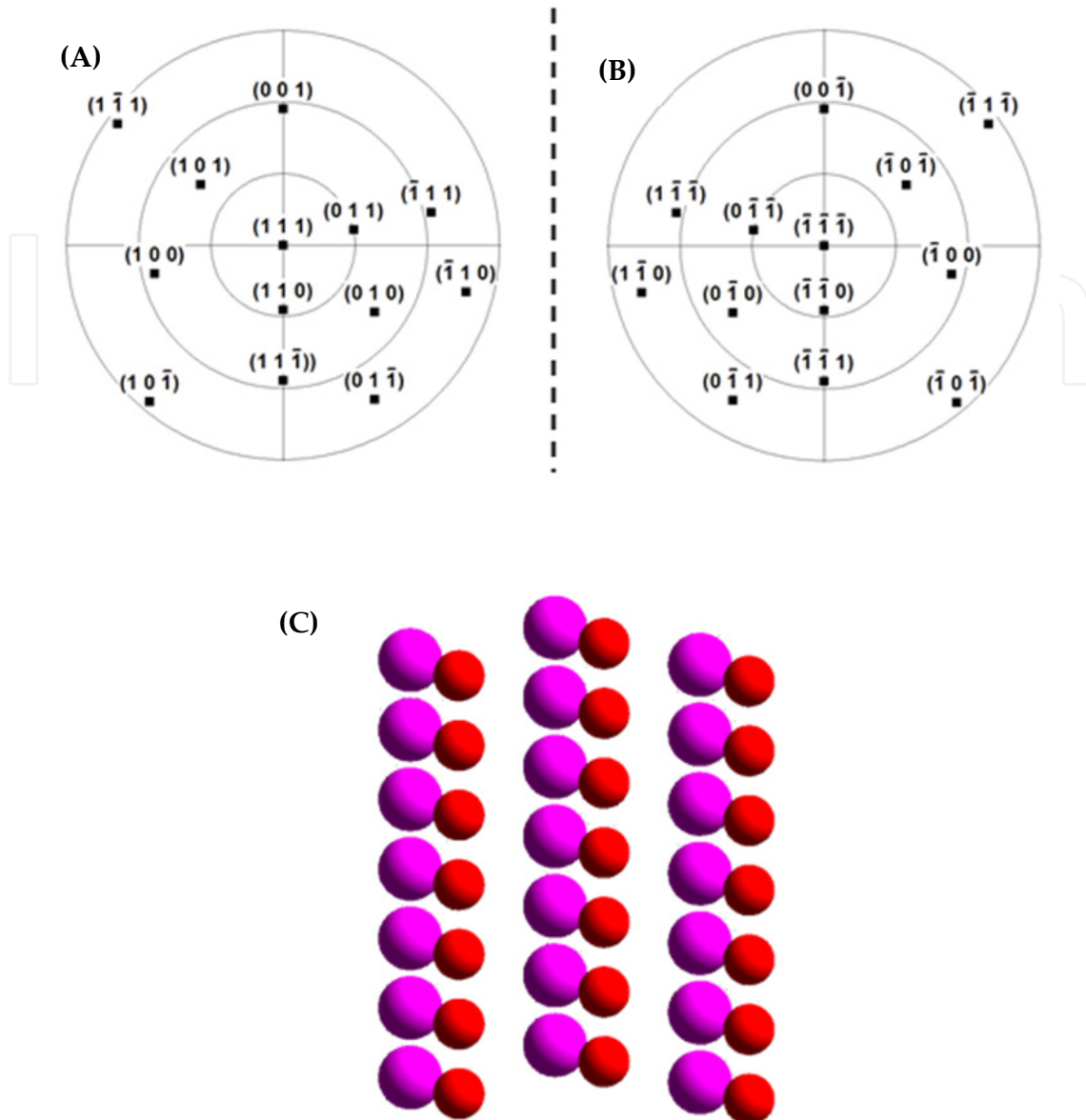
Figure 2. Stereographic projections of A) (111) and B) (-1-1-1) orientation of CuO. These two orientations are nonsuperimposable mirror images of each other; they are chiral. The radial grid lines on the stereographic projections correspond to 30° increments of the tilt angle, χ. C) the interface model of (-1-1-1) CuO (red oxygen atoms) on (111) CuO (violet oxygen atoms) with a common [1-10] direction. These two surfaces are nonsuperimposable; therefore, they are chiral.

X-ray diffraction works on the principle of Bragg's law, $n\lambda = 2d \sin \theta$, where λ is the x-ray wavelength, d is the lattice spacing and θ is the Bragg angle. The layers of a crystal act like weak reflecting mirrors for the X-rays. Only if the path difference of the reflected X-rays is a whole number of wavelengths does constructive interference occurs, as shown in Figure 3.

In general, X-ray diffraction patterns are plots of intensity versus 2θ angle. Different planes in a crystal diffract at different angles giving a pattern which is unique to a crystal. The intensities of the reflections are determined by the distribution of the electrons in the unit cell. X-rays going through areas with high electron density will reflect strongly and areas

with low electron density will give weak intensities. Therefore, every crystalline material has a unique X-ray diffraction pattern that can be used to determine the crystallinity and phase of the deposited material.

Thin films deposited on polycrystalline substrates can be analyzed by running two types of experiments. In the first case, a symmetric scan (gonio scan) can be used to evaluate the out-of-plane texture of the film. It is a conventional θ-2θ scan for the Bragg-Brentano geometry. Figure 4 (A) shows a schematic representation of a gonio scan. Where, ω is the incident angle and θ is the diffracted angle.
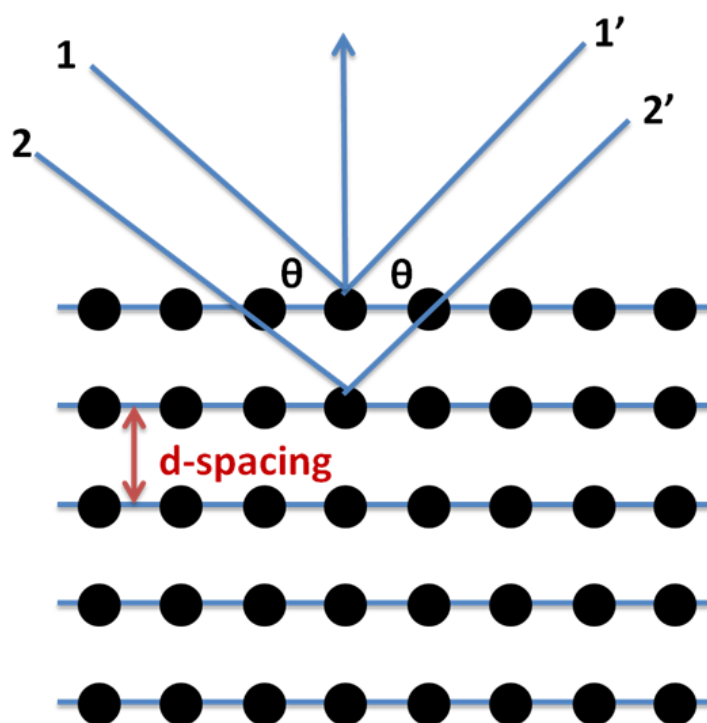
Figure 3. Schematic representation of Bragg's law.

In a gonio scan, ω = θ and ω + θ = 2θ. Another way to characterize thin films is through glancing angle measurements, as shown in Figure 4 (B). In this case, ω + θ = 2θ and ω is fixed but θ varies. Glancing angle measurement is a good technique to measure polycrystalline grains. As the w is fixed and the θ is varied, all the planes in the material are brought into the Bragg condition. However, this technique cannot be used for highly oriented films or epitaxial films.

Epitaxial films deposited on single crystals are oriented both out-of-plane as well as in-plane. In this case, X-ray characterization such as diffraction patterns, pole figures, azimuthal scans, and rocking curves are performed.

Unlike polycrystalline films, epitaxial films grow with one orientation and show only a family of planes in the pattern. In Figure 4, an epitaxial magnetite film deposited on a Ni(111) substrate shows only the {111} family peaks. [38] The experimental setup to determine out-of-plane orientation is similar to the gonio scan but instead a 2θ-omega scan

is run. The difference between this and the gonio scan is that there can be an offset between 2θ and omega, so that omega = $\frac{1}{2}$ 2θ + offset. This is useful when collecting a diffraction scan from an epitaxial film, when the tilt of the film is compensated by the offset. Identification of the pattern is done by comparing the pattern with the existing patterns in the database. For example, a magnetite film is identified by JCPDS#19-0629 pattern. However, this does not provide any information about in-plane orientation of the film. To determine the in-plane orientation of the film, X-ray pole figures and azimuthal scans are run. Pole figures can be used to probe planes which are not parallel with the geometric surface of the sample. The sample is moved through a series of tilt angles, χ, and at each tilt angle the sample is rotated through azimuthal angle, ϕ, of 0 to 360º. Peaks occur in the pole figure when the Bragg condition is satisfied. During the experiment 2θ is fixed, which is normally the highest intensity peak of a randomly oriented powder diffraction pattern of the material. Figure 6 is a schematic representation of a pole figure measurement. Azimuthal scans can be considered as a cross-section of a pole figure. They are obtained when the measurement is carried out at a specific 2θ for only specific tilt angle, χ, and rotated azimuthally, ϕ, from 0 to 360º. Comparing the azimuthal scans at specific tilt angle for a substrate and a film, we can obtain the epitaxial relationships.
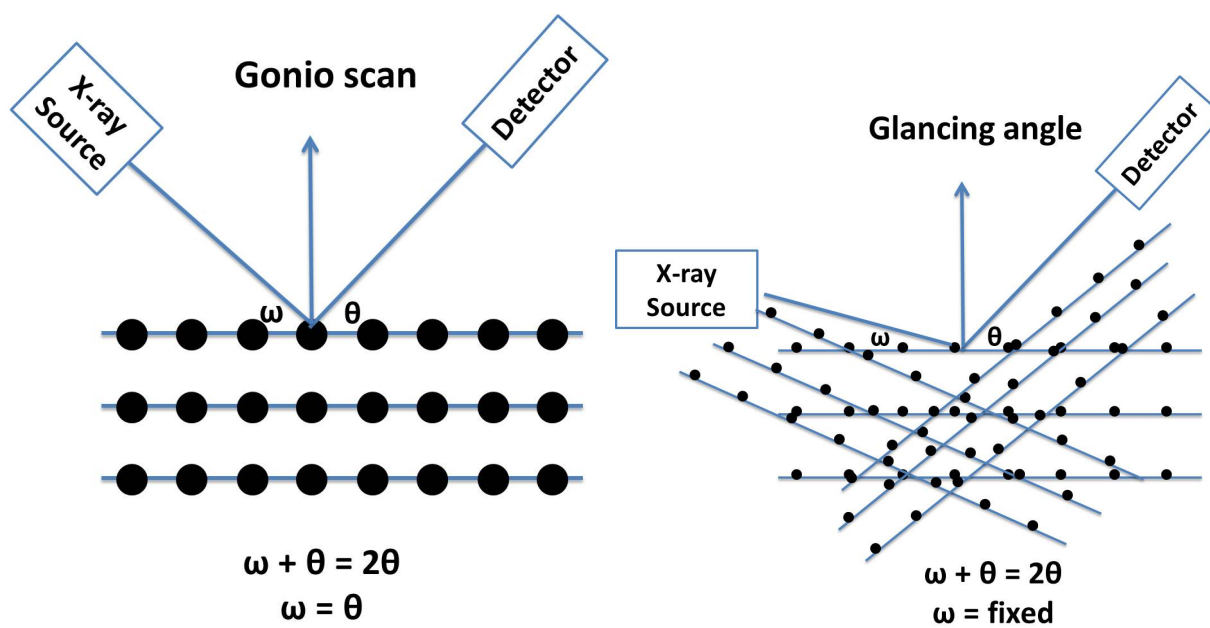
Figure 4. Schematic representation of (A) gonio scan used for textured films and (B) glancing angle used for polycrystalline grains.

To determine the quality of epitaxy, X-ray rocking curves are run. The rocking curves indicate the mosaic spread of the film relative to the substrate. The larger the full width at half maximum (FWHM), the larger the mosaic spread. In the experimental setup for a rocking curve, only the omega axis is scanned as data are collected. All other axes, such as 2θ, are fixed at specific angles. In a perfect single crystal, the FWHM is small indicating that all domains are aligned. The width of the rocking curve is a direct measurement of the range of orientation of the sample. In general, the rocking curves are performed for substrate as

well as the film for comparison of mosaic spread. If the mosaic spread of the film is low and comparable to the substrate, the peaks in the pole figure become sharper and more intense. Rocking curves have been used to understand the in-plane misorientation of ZnO, AlN, and GaN on sapphire and MgO films grown on GaAs.
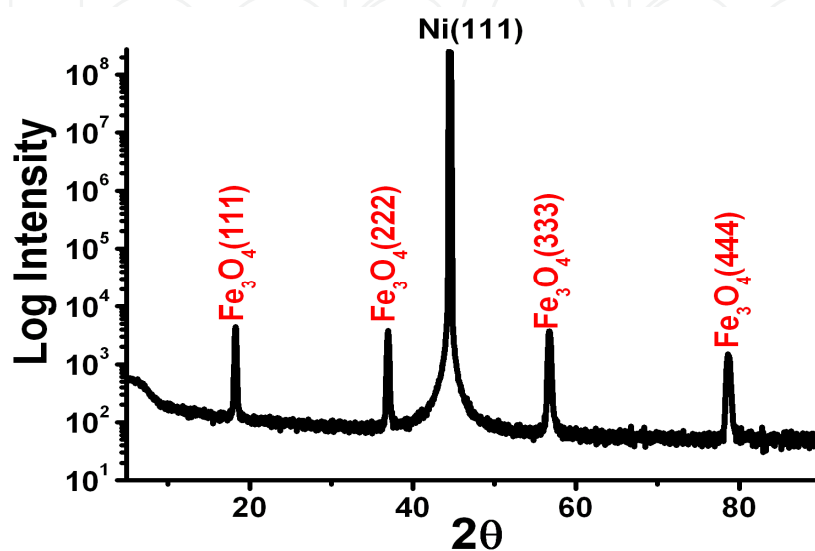

Figure 5. X-ray diffraction pattern of an epitaxial magnetite (Fe3O4) film on Ni(111) single crystal.

5. Electrodeposition of chiral films

Electrodeposition is a versatile method for depositing metals, metal oxides, semiconductors, and biomaterials. [20, 21] It is a simple and a low cost process which uses electrically conductive aqueous, organic, or fused salt solutions. Electrodeposition also offers the ability to tune the characteristics of the film by varying factors such as the electrolyte composition, the additives, the pH and temperature of the electrolyte, and the applied overpotential or current density. [40]

The most familiar method to electrodeposit a film involves electrochemically oxidizing or reducing the cation in the electrolyte at the electrode surface. In this process, the electrochemically produced species reacts with water or hydroxide ions to form a metal oxide on the electrode. [41-57] A second method to produce thin films is to electrochemically change the pH of the electrolyte at the electrode surface. Because the solubility of any material is dependent on pH, the pH can be electrochemically changed at the electrode surface, thus lowering the solubility of the material and resulting in the precipitation of the material only on the electrode surface. The pH can be decreased by electrochemically oxidizing water, ascorbates, hydroquinone, and other organics to produce metal oxides. Likewise, the pH can be electrochemically increased by reducing water, molecular oxygen, nitrate, peroxide, or organic molecules such as quinones. [58]
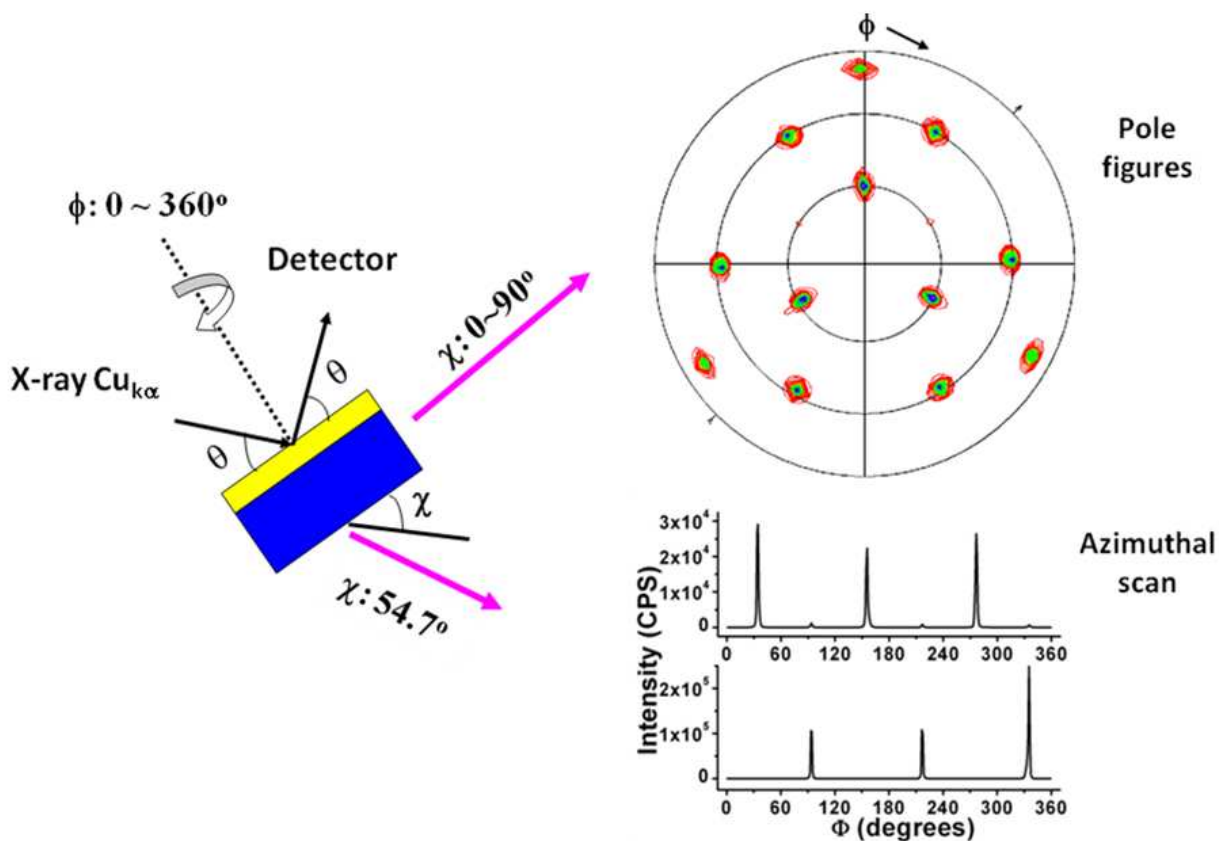
Figure 6. An illustration of the method to produce a (311) magnetite pole figure of a (111) oriented magnetite film on a Ni(111) substrate. The azimuthal scan on the bottom right is obtained by running the φ scan at a fixed χ.

Electrodeposited films orientation and morphology are determined by the electrochemical/chemical reaction, potential, current, pH, temperature, and additives. [40] For example, Switzer group has previously shown that varying the applied potential and pH changes the orientation and size of the electrodeposited Cu_2O films. [59, 60] Films follow the orientation of the substrate at low overpotentials and change to a kinetically controlled orientation at a critical thickness. As the overpotential increases, the critical thickness for the transition decreases. Similarly, Cu_2O films from a pH 9 solution have a [001] preferred orientation while films from a pH 12 solution have a [111] preferred orientation. Siegfried and Choi have examined the stability of facets of Cu_2O in the presence of additives where ammonium salts stabilize {111} planes, whereas sodium chloride stabilizes {100} planes. [61]

Thin films of metals and metal oxides can be electrodeposited on polycrystalline substrates or single crystalline substrates. Polycrystalline films grow on polycrystalline substrate and are usually used for identification and characterization. Different planes of atoms produce different diffraction peaks, which contain information about atomic arrangement within the crystal. Therefore, every crystalline material has a unique X-ray diffraction pattern. [62] This pattern can be used to determine the crystallinity and phase of the deposited polycrystalline

material. The lattice parameters of a material can be calculated from the peaks by properly assigning Miller indices (hkl) and accurately measuring the d-spacing. However, if the films are grown on single crystals such as Au(001), Au(111), Si(111), Ni(110) and InP(110) we get epitaxial films. Single crystals eliminate the presence of grains of various orientations, which may have different film growth rates as discussed above. If a crystalline film grows with an out-of-plane and in-plane orientation that is dependent on the orientation of the substrate, the film is said to be epitaxial.

The properties of epitaxial films depend on the substrate. The film will have better crystalline quality and more uniform morphology when fewer defects are present on the substrate. Generally, an epitaxial film will deposit with an orientation providing the lowest lattice mismatch with the substrate. In some cases, the film will become strained or will rotate to obtain this low mismatch. Thus, different substrates will produce different orientations of the film. Since properties of a material can be dependent on the orientation, this control over selection of orientation permits optimization of the properties of a deposited material. Epitaxial films are useful in device applications, since the intrinsic properties of the material can be exploited rather than its grain boundaries. Epitaxial films can be characterized using X-ray diffraction, pole figures, azimuthal scans, and rocking curves. For example, the diffraction pattern of a polycrystalline film is different than that of an epitaxial film. Whereas a polycrystalline film has all possible planes, resulting in multiple peaks in the pattern, an epitaxial film will normally grow with one orientation and show family of planes in the pattern. The details of X-ray characterization for epitaxial films have been discussed in the above section. [40]

Enantiospecific epitaxial thin films of CuO can be electrodeposited onto Au(100), Cu(111), and Cu(110) single crystals from alkaline solutions. [18, 19, 33] The Chirality of the electrodeposited film in alkaline bath was determined by the enantiomer used to complex Cu(II). Chiral CuO films were deposited on Au(001), Cu(111) and Cu(110) single crystals from alkaline solutions of copper(II) complexed with tartaric acid, malic acid, and amino acids. The films were deposited either at constant current density or at constant potential. The CuO films deposited on Au(001) using tartaric acid as complexing agent in the deposition bath resulted in {1-1-1} set of peaks. [18, 19] Chirality of the film cannot be determined by the θ-2θ X-ray scan. The films grown from a solution of L-tartaric acid or D-tartaric acid can have either (1-1-1) or (-111) orientations. It is impossible to distinguish between the orientations based on the θ-2θ scans as they have identical d-spacing. The orientations can be assigned with the help of X-ray diffraction pole figure. The CuO(111) pole figures and stereographic projections indicated that the films grown from L-tartaric acid has (1-1-1) orientation whereas the film grown from D-tartaric acid has (-111) orientation. These two stereographic projections are non-superimposable mirror images of each other. The enantiomeric excess of one orientation over the other was determined from azimuthal scans probing the higher angle CuO (111)-type reflections. The percentage enantiomeric excess for the (1-1-1) orientation can be calculated quantitatively from the area under all the peaks obtained at higher angle using the formula.

$$ee = (A_{(1\text{-}1\text{-}1)} - A_{(\text{-}111)}/A_{(1\text{-}1\text{-}1)} + A_{(\text{-}111)}) *100$$

For a film deposited from L-tartaric acid has an enantiomeric excess of 95% while the films deposited from D-tartaric acid has an enantiomeric excess of 93%. The film from DL-tartaric acid has equal amounts of both the orientations and zero enantiomeric excess. For the CuO films grown from alkaline solutions using amino acids on Au(001) resulted in {1-1-1} and {-111} orientations. The films were grown with the alkaline amino acids solutions of alanine, valine, and glycine. The films grown from Cu(II) complexes of amino acids have two chiral orientations with a smaller enantiomeric excess. The films grown from L-alanine and L-valine solutions have a small excess of (-111) and (-1-1-1) orientations, while the films grown from D-alanine and D-valine have a small excess of the (1-1-1) and (111) orientations. The pole figures obtained from achiral glycine as a complexing agent have equal amounts of the chiral CuO(-111) and CuO(1-1-1) orientations.

For the films grown from Cu(II) complexes of malic acid on Cu(111) single crystals, two chiral orientations were obtained. The films produced from L-malate in the deposition bath have (-111) and (311) orientations and the ones produced from D-malate have (1-1-1) and (-3-1-1) orientations. CuO films grown on Cu(110) from L-malate had (110) and (31-1) orientations while the one grown from D-malate deposition bath had (-1-10) and (-3-11) orientations. The films grown from racemic malate showed equal amounts of only (-111) and (1-1-1) orientations on Cu(111) and CuO(110) and CuO(-1-10) orientations on Cu(110) single crystal. It is still not clear as to why the CuO films grown from malic acid in the deposition bath show 2 chiral orientations where as the films grown from tartaric acid show only one dominant chiral orientation. One argument can be that in a strong alkaline solution that the crystal structure of chiral Cu(II) malate has a different packing than the racemix Cu(II) malate. It is difficult to grow crystals of Cu(II) malate or Cu(II) tartarate from highly alkaline solutions. To understand the phenomenon of chiral electrodeposition, the crystals of copper(II) malate were grown at pH=1.5. Both L- and D- chiral complexes polymerize in a similar fashion where each copper is coordinated to two malate ligands of the same chirality via one hydroxyl oxygen atom and one carboxyl oxygen atom. Both the chiral complexes crystallized in P2$_1$ monoclinic space group. Whereas the complxes grown from racemic Cu(II)-malate crystallized in a centrosymmetric space group P21/c with copper atoms at the inversion center. Similarly, other copper(II) complexes have structures which are determined by the handedness of the ligand. It is believed that the chiral complexes formed in the solution are initially adsorbed on the surface and imprint chirality on the surface. However, further study has to be done to understand this phenomenon better.

To get a better understanding for the chiral electrodeposition further studies were done by growing CuO films on Cu(111) single crystal with different amino acids in the solution bath. Table 2 shows different chiral reagents used for depositing CuO films. The table also indicates their handedness in different conventions.[1] Usually, there are three different types of conventions which are followed for chiral molecules. Optical activity (+/-) is based on the direction in which the enantiomer rotates the plane polarized light. The (+) and (-) enantiomer are also identified as dextrorotatory (d) and levorotatory (l). This notation can be easily confused with D and L labeling. The D/L labeling is unrelated to +/- notation; it does

indicate which enantiomer is dextrorotatory or levorotatory. Rather, it says that the compound's stereochemistry is related to the stereochemistry of the dextrorotatory and levorotatory enantiomer of glyceraldehydes. Another convention which is generally used is the R/S configuration. In this convention, each chiral center in the molecule is either named R or S according to a system by which its substituent's are each assigned a priority. The priorities are based on Cahn Ingold Prelog rules, based on atomic number. The R/S system has no fixed relation with +/- or D/L systems. An R isomer can be either dextrorotatory or levorotatory, depending on its exact substituents. [63]

Amino Acids	*(+) /(-) notation*	*d/l – notation*	*D/L-notation*	*R/S-Notation*
Alanine	+	d	L	S
Arginine	+	d	L	S
Asparatic acid	-	l	L	S
Glutamic acid	+	d	L	S
Valine	-	l	L	S
Tartaric acid	+	d	L	R, R
Malic acid	-	l	L	S
Proline	-	l	L	S

Table 2. List of chiral precursors used for depositing CuO on Cu(111) single crystal. The table also lists different types of notations used for chiral molecules.

In this work, different chiral reagents were used to deposit CuO films on Cu(111) single crystals to understand the role of the precursor on chiral film formation. Figure 7 shows the (111) pole figures for CuO on Cu(111) deposited from different chiral reagents. The pole figures were obtained by setting 2θ equal to the angle of diffracted intensity for the (111) planes ($2\theta = 38.742°$) and performing azimuthal scans at tilt angles, χ, from 0 to 90°. The pole figures in Figure 7 (A) - (E) show peaks at 57° and 63°. These peaks correspond to either (-111) orientation or (1-1-1) orientation. On the other hand, the pole figures in Figures 7 (F) – (H) have extra peaks at tilt angle of 27°, which correspond to either (311) or (-3-1-1) orientation. To interpret pole figures, we use stereographic projections. Figures 8(A) and 8(B) shows the (-111) and (1-1-1) stereographic projections of monoclinic CuO. The radial direction is the tilt angle, χ, while the azimuthal angle, ϕ, is the rotation of the sample about the axis. The positions of CuO{111} and CuO{200} reflections are specified. Figure 8(A) shows that for the (-111) orientation, reflections from the (-11-1) plane at a χ of 57°, and the (111) planes at a χ of 63°, are separated azimuthally by 115° rotated counterclockwise ($\Delta\phi$ = -115°). Figure 8(B) shows that for (1-1-1) orientation, reflections from the (1-11) plane at χ = 57° and the (-1-1-1) plane at χ = 63° are separated azimuthally by 115° rotated clockwise ($\Delta\phi$

= 115°). The calculated interplanar angles obtained from stereographic projections correspond with the measured interplanar angles of the pole figures. Figure 7 (F)-(H) also show reflections at $\chi = 27°$. These reflections can be explained by figures 8(C) and 8(D). Figure 8(C) shows that for the (311) orientation, reflections from the (111) plane at a χ of 27.19°, and the (1-11) plane at a χ of 68.14°, are separated azimuthally by 125.18° rotated counterclockwise. Figure 8(D) shows that for the (-3-1-1) orientation, reflections from the (-1-1-1) plane at χ of 27.19°, and the (-11-1) plane at a χ of 68.14°, are separated azimuthally by 125.18° rotated clockwise. Figures 8(A) and 8(C) clearly explains the pole figure of Figure 7 (F)-(H) and confirms the presence of (-111) and (311) orientations for the film grown from different amino acid deposition bath. Similarly, Figures 8(A) and 8(B) explain the pole figure of Figure 7 (A)-(E) and confirm the presence of (1-1-1) and (-111) orientations.

Figure 9 shows the SEM images of the CuO films deposited on Cu(111) single crystal from different chiral reagents. The chiral reagents influence the morphology of the deposited films. Figure 9 (D) shows the SEM image of the CuO film deposited using L-asparatic acid precursor. The image shows that CuO grows like spears and are approximately 50 nm in diameter. On the other hand, films deposited using L- arginine has cross hatch morphology with individual crystallites made up of multiple platelets. The morphology of the films deposited from other amino acids and simple carboxylic acids like malic acid and tartaric acid have simple cross hatch morphology with different crystallite sizes.
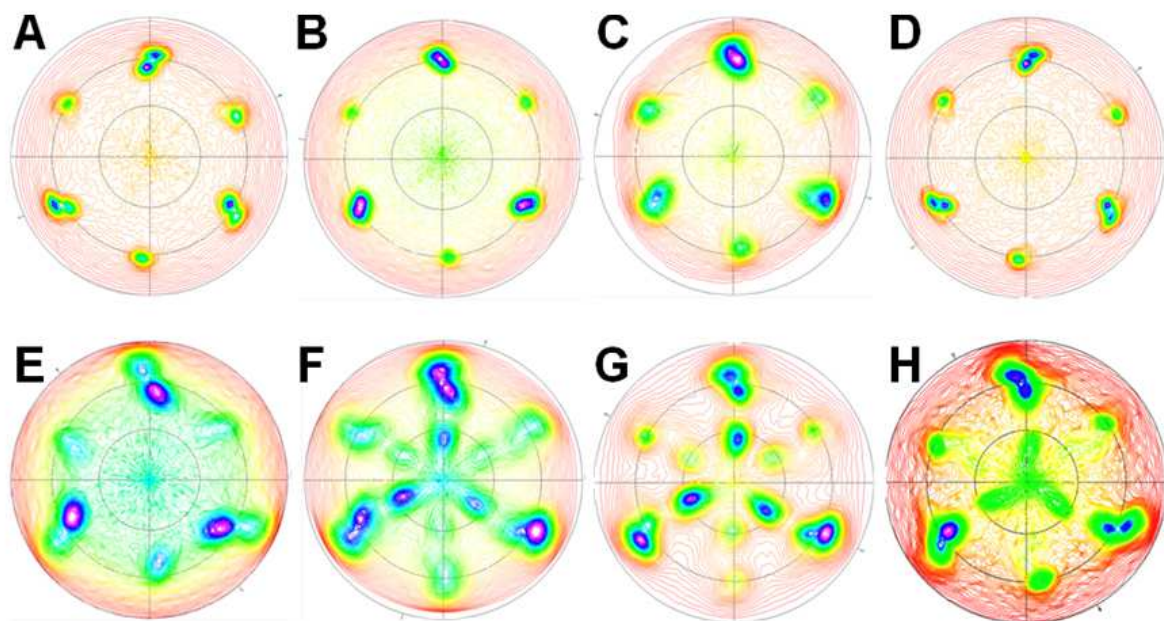
Figure 7. (111) CuO pole figure for CuO films deposited from different amino acids on Cu(111)single crystals. (A) tartaric acid, (B) asparatic acid, (C) glutamic acid, (D) proline, (E) arginine, (F) alanine, (G) valine and (H) malic acid.

The scanning electron microscopy (SEM) does not correlate the handedness of the electrodeposited films with their microstructure. However, the SEM images of the electrodeposited biominerals show very clearly the effect of additives in the solution. Different additives in the solutions are known to cause face-selective crystallization of inorganic crystals in biosystems. It was recently shown that in presence of chiral precursors, calcite and other biominerals with chiral morphology can be electrodeposited. [29] A combination of geometric matching, electrostatic interactions and stereochemistry is believed to be the cause of bimonineralization. [64] Researchers have shown that in the presence of chiral amino acids, asymmetric crystals of gypsum can be crystallized. [28] In nature, gypsum crystallizes in symmetric space group but by changing the solution precursors systematically one can control the handedness of the crystallites. Other researchers have studied the affect of step-edge free energies for the formation of chiral etch pits. [26]
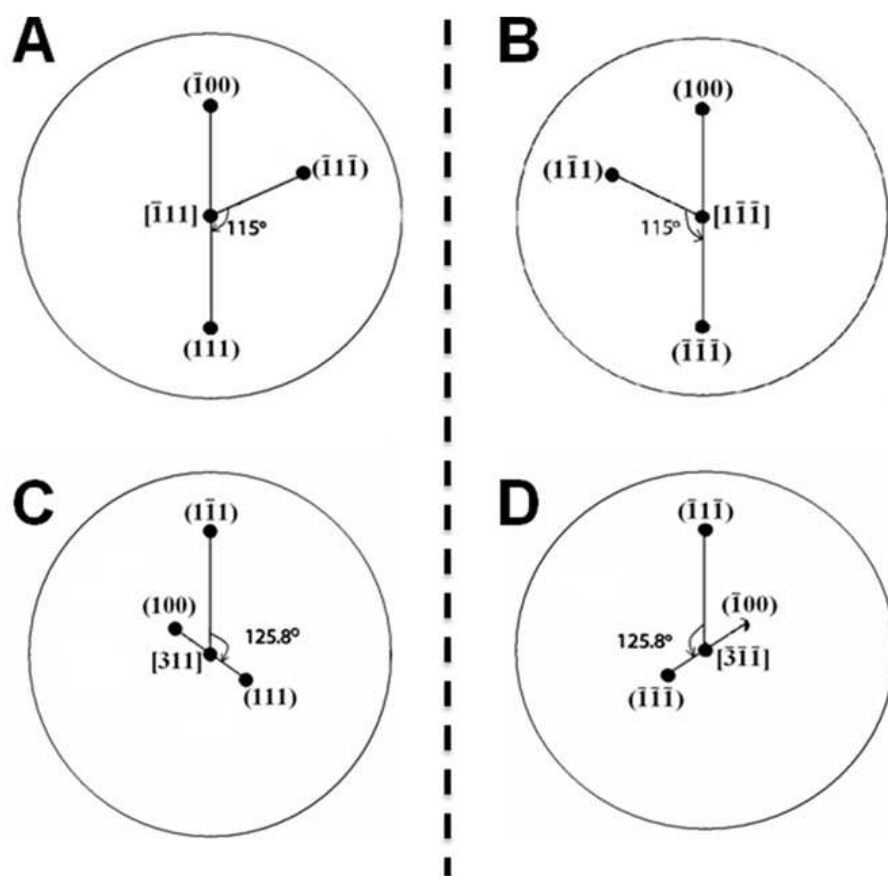
Figure 8. Stereographic projections for (A) (-1-11), (B) (11-1), (C) (311) and (D) (-3-1-1) orientations indicating the positions where the (111) type and (100) type reflections should be observed in the pole figures. For the   (-1-11) orientation, reflections from the (1-11) plane at $\chi = 57°$ and the   (-1-1-1) plane at $\chi = 63°$ are separated azimuthally by 115° rotated counterclockwise. For the (-3-1-1) orientation the (1-11) plane is at $\chi = 68.14°$, the (-1-1-1) planes at $\chi = 27.41°$ and (100) planes at $\chi = 27.19°$. For the (11-1) orientation the (-11-1) plane is at $\chi = 57°$ and the (111) plane is at $\chi = 63°$ are separated azimuthally by 115° rotated clockwise. For the (311) orientation the (1-11) plane at $\chi = 68.14°$, the (111) plane at $\chi = 27.41°$ are separated azimuthally by 125.8°.

Surface templating and imprinting can be the two main ways of obtaining chiral surfaces. Studies have shown that adsorption of chiral tartaric acid on low index surfaces of Cu and Ni can break the symmetry of the substrate causing chiral templates. On the other hand, adsorption of (R,R)-tartaric acid on Ni(110) surfaces results in chiral imprinting. [6] The difference between the two can be best described as following, in the case of chiral imprinting; the adsorbed molecule irreversibly reconstructs the substrate, whereas in the case of templating; the underlying substrate is not affected upon the removal of adsorbed molecule.
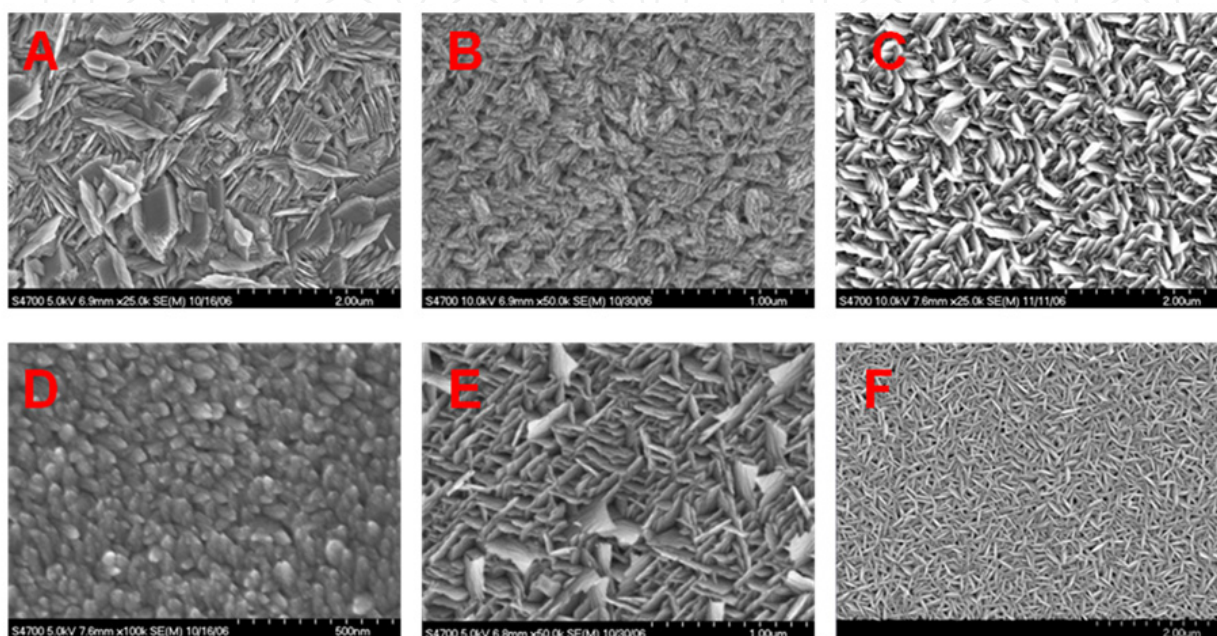

Figure 9. SEM micrographs for CuO films deposited on Cu(111) single crystal from different chiral precursors. (A) L(+)-Alanine, (B) L(-)-Arginine, (C) L(+)-Valine, (D) L(-)-Aspartic acid, (E) L(+)-Glutamic acid

In the case of electrodeposited chiral CuO films, it would not be unreasonable to expect chiral Cu(II) complexes to adsorb on the single crystal surfaces and break its symmetry. As discussed earlier, complexes of copper(II) with different chiral reagents have a dimeric structure with a symmetry that is determined by the handedness of the ligands. Surface reconstruction of the underlying single crystal substrate from adsorbed molecules can be another cause for the asymmetry. The precise mechanism, however, is not known at this time. Studies have shown that presence of chiral modifiers is necessary for the nucleation of chiral CuO domains. Once the nucleation layer is produced, the film maintains the orientation regardless of the precursor. [47] Studies on adsorption of organic molecules on surfaces have shown that local chiral imprinting can be obtained without the need of extended surface Chirality. [6] Adsorption of amino acids on Au [66] and Ag [67] surfaces are reported to be physical in nature, while amino acids chemisorb on Cu single crystals. Based on this argument the films grown on Cu single crystals should have more order as compared to other crystals. We have shown in this study that this is indeed true. To get more insight into the mechanism of chiral electrodeposition, further investigation is required. In-situ AFM during the chiral electrodeposition can be helpful in understanding the initial nucleation and whether or not it is local chiral imprinting which results in chiral films.

An interesting aspect of the electrodeposited chiral films is that they show chiral selectivity. [18, 19] In this process, the chiral film selectively oxidizes the chiral molecules in the solution. This property of the chiral films can be utilized post enantiomeric separation to detect the amount of enantiomeric excess in the mixture.

6. Electrochemical selectivity

Researchers have studied the electrochemical oxidation of sugars on chiral Pt surfaces. [15] In this study, enantiospecific electrochemical oxidation of glucose was demonstrated on Pt(643) and Pt(-6-4-3) surfaces. Recent studies show that chiral cyclodextrin based coatings applied to a three-transducer microsystem shows distinct chiral discrimination for different compounds. [68] CuO has been shown to be catalytic for the electrochemical oxidation of amino acids, carbohydrates and amines with very high sensitivities. [69-71] It has been reported that increased sensitivity for the electroxidation of amino acids with an increase in solution pH. [72] Electrodeposited chiral CuO films also show chiral selectivity in high pH chiral solutions. [18] It was shown that the film grown from L-tartaric acid selectively oxidizes L-tartaric acid over D-tartaric acid, whereas the films grown from D-tartaric acid does the opposite. For the films grown from a racemic tartaric acid, no selectivity was observed.
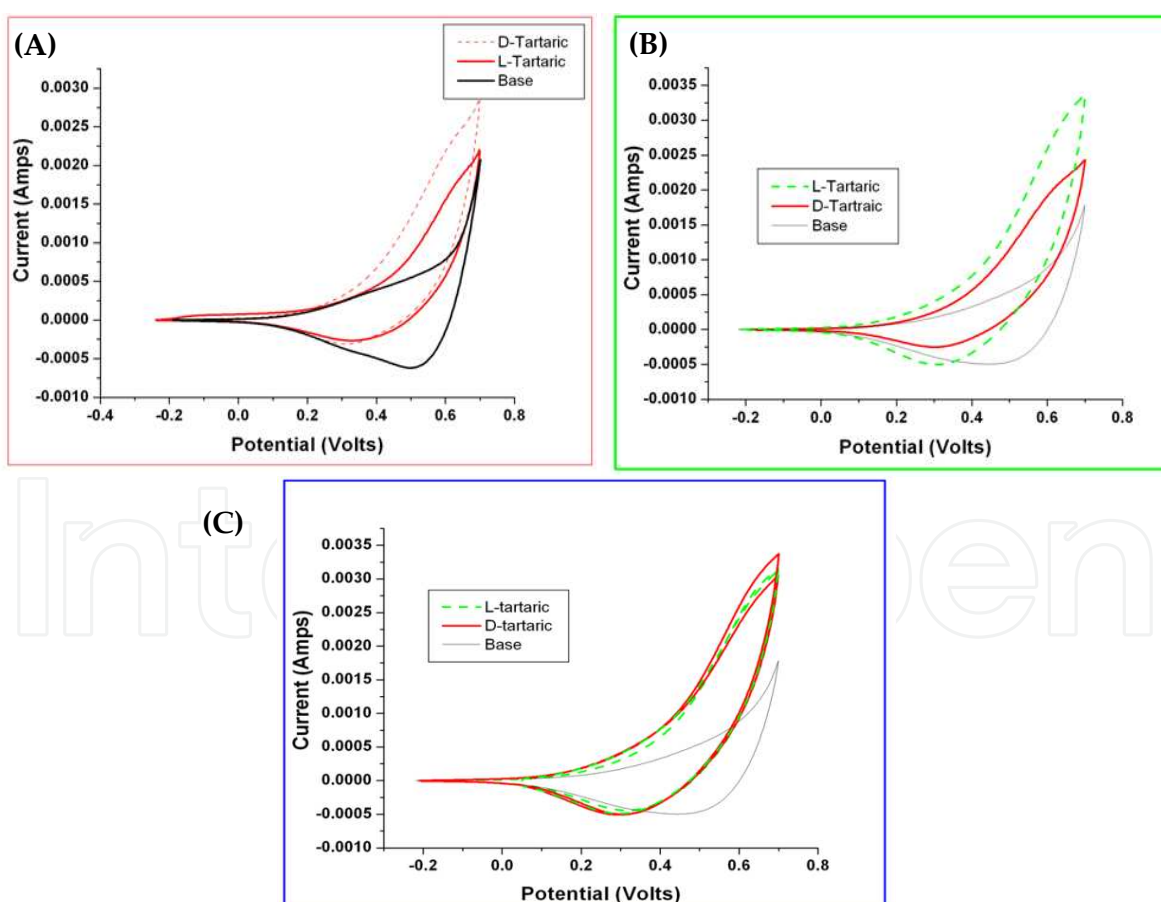
Figure 10. Cyclic voltammograms in unstirred solutions of alkaline solutions of L-, D-, and DL- tartaric acid by scanning from open circuit potentials to 0.75 V vs. SCE at a scan rate of 10 mV/sec for the films grown (A) L-malic acid, (B) D-malic and (C) DL-malic acid

The study was extended to understand the selectivity behavior of a chiral film deposited with malic acid precursor and oxidizing tartaric acid films. The cyclic voltammograms (CV) were obtained in unstirred solutions by scanning from open circuit potentials to 0.75 V vs. SCE at a scan rate of 10 mV/sec. Before switching solutions the electrode was cleaned by scanning in 0.1 M NaOH from the OCP to 0.75 vs. SCE to remove adsorbed remnants from the electrode. Figure 10(A) shows the film grown from L-malic acid selectively oxidizes for D-tartaric acid, whereas the Figure 10 (B) film grown from D-malic acid does the opposite. Figure 10 (C) shows for the film grown from racemic malate has a very slight selectivity for D-tartaric acid but it is insiginificant difference compared to the selectivity shown by the chiral films. This study is in agreement with the pole figures for the CuO films grown on Cu(111) single crystals from the solutions of malic and tartaric acid precursors. The CuO films grown from D-malic acid and L-tartaric acid have similar dominant orientations and hence the similar selectivity. Another study has shown that by selectively etching the chiral CuO films the selectivity can be enhanced considerably. However, a detail study on more complex molecules still needs to be studied to validate this model. The final goal should be to have a sensor grown from one chiral molecule which can selectively distinguish any chiral molecule with the same handedness.

In summary, enantiospecific epitaxial CuO films can be electrodeposited onto single crystal substrates from copper (II) complexes of chiral molecules. Chirality of a crystal is dependent on the symmetry operations in the structure. Chirality can be imparted to non chiral crystals by depositing the films in the presence of chiral precursors. The chiral orientation of the films can be determined by X-ray pole figures and stereographic projections. The chiral CuO films show selectivity in the alkaline chiral solutions. At this point, the mechanism of the chiral electrodeposition is not very well understood and needs further study.

Author details

Rakesh Gudavarthy
Missouri University of Science and Technology, Rolla, Missouri, USA Current address: Intel Corporation, Hillsboro, OR, USA

Elizabeth A. Kulp
Missouri University of Science and Technology, Rolla, MO, USA

Acknowledgement

7. References

[1]   Rouhi, A.M. Chem. Eng. News 2004; 82, 47.

[2] Rentsch K. M. The importance of stereoselective determination of drugs in the clinical laboratory. Journal of Biochemical and Biophysical Methods 2002; 54(1-3), 1-9.

[3] Walther W, Netscher T. Design and Development of Chiral Reagents for the Chromatographic Determination of Chiral Alcohols. Chirality, 1996; 8, 397-401.

[4] Katzung B. G. The Nature of Drugs. In: Basic and Clinical Pharmacology. 9th Ed. New York, Lange Medical Books/McGraw Hill, 2004; 3-5.

[5] Stinson S. C. Chiral Pharmaceuticals. Chem. Eng. News 2001; 79, 79–97

[6] Lorenzo M. O, Baddeley C. J, Muryn C, Raval R Nature 2000; 404, 376–379.

[7] Humblot V, Haq S, Muryn C, Hofer W. A, Raval R. J. Am. Chem. Soc. 2002; 124, 503–510.

[8] Kühnle A, Linderoth T. R, Hammer B, Besenbacher F. Nature 2002; 415, 891–893.

[9] Izumi Y. Advances in Catalysis 1983; 32, 215–271.

[10] LeBlond C, Wang J, Liu J, Andrews A. T, Sun Y. K. J. Am. Chem. Soc.1999; 121, 4920–4921.

[11] McFadden C. F, Cremer P. S, Gellman A. J. Langmuir 1996; 12, 2483–2487.

[12] Horvath J. D, Gellman A. J. J. Am. Chem. Soc. 2001; 123, 7953–7954.

[13] Horvath J. D, Gellman A. J. J. Am. Chem. Soc. 2002; 124, 2384–2392.

[14] Ahmadi A, Attard G, Feliu J, Rodes A. Langmuir 1999; 15, 2420–2424.

[15] Attard G. A. J. Phys. Chem. B 1999; 103, 1381–1385.

[16] Attard G. A. J. Phys. Chem. B 2001; 105, 3158–3167.

[17] Sholl D. S, Asthagiri A, Power T. D. J. Phys. Chem. B 2001; 105, 4771–4782.

[18] Switzer J. A, Kothari H. M, Poizot P, Nakanishi S, Bohannan E. W. Nature 2003; 425, 490.

[19] Kothari H. M, Kulp E. A, Boonsalee S, Nikiforov M. P, Bohannan E. W, Poizot P, Nakanishi S, Switzer J. A. Chem. Mater. 2004; 16, 4232.

[20] Switzer J. A, Electrochemistry of Nanomaterials, G. Hodes, Ed. Wiley-VCH, Weinheim 2001; chap 3.

[21] Switzer J. A. Handbook of Nanophase Materials, A. Goldstein, Ed. Marcel Dekkar, New York 1996; chap 4.

[22] Hazen R. M, Sholl D. S. Nat. Mater 2003; 2, 367.

[23] Orme C. A, Noy A, Wierbicki A, McBride M. T, Grantham M, Teng H. H, Dove P, De Yoreo J. J. Nature 2001; 411, 775.

[24] Addadi L, Weiner W. Nature 2001; 411, 753.

[25] Teng H.H, Dove P. M, Orne C. A, De Yoreo J. J. Science 1998; 282, 724.

[26] Cody A. M, Cody R. D. J. Cryst. Growth 1991; 113, 508.

[27] Aizenberg J, Black A. J, Whitesides G. M. Nature 1999; 398, 495.

[28] Hazen R. M, Filley T. R, Goodfriend G. A. Proc. Natl. Acad. Sci. USA 2001; 98, 5487.

[29] Kulp E. A, Switzer J. A. J. Am. Chem. Soc. 2007; 129, 15120.

[30] Challener C.A. Overview of Chirality. In: Chiral Drugs. 1st Ed. Aldershot (England), Ashgate Publisher 2001; 3-14.

[31] Drayer D.E. The Early History of Stereochemistry. In: Drug Stereochemistry. Analytical Methods and Pharmacology. 2nd Ed., Wainer I. W, Editor. New York, Marcel Dekker Publisher 1993. P 1-24.

[32] Reddy I. K, Mehvar R, Chirality in Drug Design and Development, Marcel Dekker, Inc; 2004.

[33] Gudavarthy R. V, Burla N, Kulp E. A, Limmer S. J, Sinn E, Switzer J.A. J. Mater. Chem. 2011; 21, 6209-6216.

[34] Glusker J. P, Lewis M, Rossi M. Crystal Structure Analysis for Chemists and Biologists, Wiley, New York; 1994.

[35] Henry N. F, Londsdale K. International Tables for X-ray Crystallography Vol. 1, Kynoch, Birmingham; 1952. p37-38.

[36] Whaites E, Roderick C. Essentials of Dental Radiography and Radiology 2002; 19-22.

[37] Culity B. D, Stock S. R. Elements of X-ray Diffraction, 3rd Ed. Upper Saddle River, New Jersey: Prentice Hall; 2001.

[38] Gudavarthy R. V, Gorantla S, Mu G, Kulp E. A, Gemming T, Eckert J, Switzer J. A. Chem. Mater. 2011; 23 (8), 2017–2019.

[39] Srikanth V, Speck J. S, Clarke D. R. J. Appl. Phys. 1997; 82, 4286.

[40] Switzer J. A, Hodes G, MRS Bulletin 2010; 35, 743.

[41] Liu R, Bohannan E. W, Switzer J. A, Oba F, Ernst F. Appl. Phys. Lett. 2003; 83, 1944.

[42] Liu R, Oba F, Bohannan E. W, Ernst F, Switzer J. A. Chem. Mater. 2003; 15, 4882.

[43] Liu R, Kulp E. A, Oba F, Bohannan E. W, Ernst F, Switzer J. A. Chem. Mater. 2005; 17, 725.

[44] Sorenson T. A, Morton S. A, Waddill D. G, Switzer J. A. J. Am. Chem. Soc. 2002; 124, 7604.

[45] Kothari H. M, Kulp E. A, Limmer S. J, Poizot P, Bohannan E. W, Switzer J. A. J. Mater. Res. 2006; 21, 293.

[46] Mitra, S, Poizot P, Finke A, Tarascon J. M. Adv. Funct. Mater. 2006; 16, 2281.

[47] Kulp E. A, Kothari H. M, Limmer S. J, Yang J, Gudavarthy R. V, Bohannan E. W, Switzer J. A. Chem. Mater. 2009; 21, 5022.

[48] Switzer J. A, Shumsky M. G, Bohannan E. W, Science 1999; 284, 293.

[49] Bohannan E. W, Jaynes C. C, Shumsky M. G, Barton J. K, Switzer J. A, Solid State Ionics 2000; 131, 97.

[50] Kulp E. A, Limmer S. J, Bohannan E. W, Switzer J. A. Solid State Ionics 2007; 178, 749.

[51] Breyfogle B. E, Hung C. J, Shumsky M. G, Switzer J. A. J. Electrochem. Soc. 1996; 143, 2741.

[52] Switzer J. A. J. Electrochem. Soc.1986; 133, 722.

[53] Van Leeuwen R. A, Hung C. J, Kammler D. R, Switzer J. A. J. Phys. Chem. 1995; 99, 15247.

[54] Vertegel A. A, Bohannan E. W, Shumsky M. G, Switzer J. A. J. Electrochem. Soc.2001; 148, C253.

[55] Mu G, Gudavarthy R. V, Kulp E. A, Switzer J. A. Chem. Mater. 2009; 21, 3960.

[56] Boonsalee S, Gudavarthy R. V, Bohannan E. W, Switzer J. A, Chem. Mater.2008; 20, 5737.

[57] Switzer J. A, Gudavarthy R. V, Kulp E. A, Mu G, He Z, Wessel A. J. Am. Chem. Soc. 2010; 132, 1258.

[58] Limmer S. J, Kulp E. A, Bohannan E. W, Switzer J. A. Langmuir 2006; 22, 10535.

[59] Liu R, Oba F, Bohannan E. W, Ernst F, Switzer J. A. Chem. Mater. 2003; 15, 4882.

[60] Golden T. D, Shumsky M. G, Zhou Y, VanderWerf R. A, Van Leeuwen R. A, Switzer J. A, Chem. Mater. 1996; 8, 2499-2504.

[61] Siegfried M, Choi K. S, Angew. Chem. Int. Ed. 2005; 44, 3218-3223.

[62] Cullity B. D. Elements of X-ray Diffraction, Addison-Wesley, Reading, 2nd Ed; 1978.

[63] Eliel E. L, Wilen S. H. The Stereochemistry of Organic Compounds, Wiley-Interscience; 1994.

[64] Mann S. Nature 1998; 332, 119-124.

[65] Gellman A. J, Hovarth J. D, Buelow M. T. J. Mol. Catal. A 2001; 167, 3.

[66] Zhao X, Yan H, Zhao R. G, Yang W. S. Langmuir 2002; 18, 3901.

[67] Zhao X, Yan H, Tu X, Zhao R.G, Yang W.S. Langmuir 2003; 19, 5542.

[68] Kurzawski P, Schurig V,   Hierlemann A, Anal. Chem.2009; 81, 9353-9364.

[69] Wels B, Johnson D.C. J. Electrochem. Soc. 1990, 137, 2785.

[70] Xie Y., Huber C.O., *Anal. Chem* 1991, 63, 1714.

[71] Kano K., Torimura M., Esaka Y, Goto M, J. Electroanal. Chem. 1994; 372, 137.

[72] Labuda J, Meister A, Glaser P, Werner G. Fresenius J. Anal. Chem. 1998; 360, 654.